Geometry and Static Flow Effects on Acoustic Radiation from Ducts

Richard J. Silcox*
NASA Langley Research Center, Hampton, Virginia

An experimental study of the effects of geometry, flow, frequency, and source structure on the radiation and reflection of sound from duct inlets has been conducted. This work extends a previous study by comparing two inlet shapes typical of static and flight testing and by considering higher-order radial modes. Measurements of the internal and radiated acoustic fields are presented in terms of modal reflection coefficients and absolute radiated pressure directivity. Results indicate that geometry effects associated with these practical inlet shapes become less important for a fixed cutoff ratio as the mode order and frequency are increased. Also, static inflow, while reducing the reflected wave amplitude, is shown to have little effect on radiation directivity regardless of inlet geometry.

Nomenclature

$A^{\pm}_{mn}$ = complex modal amplitude coefficient, Eq. (3)
a = radius of uniform duct sections, 0.15 m
c_0 = ambient speed of sound
J_m = Bessel function of first kind and order m
j = $\sqrt{-1}$
k = free space wavenumber, ω/c_0
ka = nondimensional frequency
M_0 = average flow Mach number in duct
m, n = azimuthal and radial mode indices, respectively; (0,0) is plane wave
p = complex acoustic pressure, Eq. (3)
R = complex pressure reflection coefficient, A^{-}_{mn}/A^{+}_{mn}
r, θ, x = cylindrical coordinates
r_w = radial coordinate of wall, Eqs. (1) and (2)
t = time
λ_{mn} = hard wall radial eigenvalues such that $J'_m(\lambda_{mn}a) = 0$
ξ = cutoff ratio, $k/\lambda_{mn}\sqrt{1 - M_0^2}$
ψ = far-field radiation angle measured from duct axis, Fig. 1
$\Omega^{\pm}_{mn}$ = modal propagation constants, Eq. (4)
ω = circular frequency

Introduction

NOISE radiated from the inlets of aircraft engines has become an increasingly important acoustic problem with the progress made in reducing jet noise. Within the scope of this overall problem an increased emphasis on the effect of both inlet geometry and flow on the radiated acoustic levels has arisen from the earlier work of Rice et al.[1] as evidenced by recent experimental work.[2,3] These works, showing significant inlet geometry effects, have generated renewed interest in analytical modeling of the radiation problem for arbitrary geometries and flow.[4,5] Additional interest has been generated by the current work in simulating the in-flight fan noise by static ground testing.[6] This work typically involves ground testing with a bellmouth inlet geometry[7] for which serious geometry effects are perceived to exist when compared to flight inlet geometries. The study of Baumeister and Horowitz,[8] an application of the work of Horowitz et al.,[4] examines both the in-flight vs static flow effects and the lip geometry effect on the radiated acoustic field.

Presented as Paper 83-0713 at the AIAA Sixth Aeroacoustics Conference, Atlanta, Ga., April 11-13, 1983; submitted April 13, 1983; revision received Oct. 25, 1983. This paper is declared a work of the U.S. Government and therefore is in the public domain.

*Aerospace Engineer, Noise Propagation and Suppression Branch, ANRD. Member AIAA.

The work of Ville and Silcox[2] was an experimental program to investigate the inlet geometry and flow effects on two simple geometries, an unflanged duct and a bellmouth inlet. This work demonstrated strong geometry effects induced by the differences in inlet contour. It also showed that flow into the bellmouth inlet under static conditions had little effect on radiation directivity although it had a strong effect on the in-duct acoustics. The present experimental program is an extension of that previous work and considers a typical flight inlet contour in addition to the bellmouth tested previously. This comparison of geometries is especially relevant in light of the current interest in simulating in-flight noise sources with static ground testing. In addition, questions arising from the use of the bellmouth inlet to determine static inflow effects on radiation directivity are investigated using the flight inlet contour. The questions relate to the idea that the long and gradual contraction rate of the bellmouth lip may have masked flow-induced directivity effects. In addition, it should be noted that the much stronger spatial mean flow gradients associated with the flight inlet under static test conditions are a more severe test of these effects under question. It is stressed, however, that the flow effects were examined only under static inflow conditions and in no way were meant to simulate the flight condition.

Thus, it is the purpose of this paper to examine the differences between these two practical geometries on the internally reflected and externally radiated acoustic fields. The effects of static inflow on the above quantities for both geometries will be shown in addition to extending the range of source functions to include higher order radial modes. An auxiliary purpose is to provide a data base of duct inlet reflection and radiation data in absolute levels for the evaluation of various analytical predictions[4,5] presently available.

Experimental Setup and Measurement Procedure

The NASA Langley spinning mode synthesizer (SMS)/flow duct facility was used to generate and propagate turbomachinery-type noise to study the reflection and radiation characteristics of two inlet geometries. The test conditions included inlet flow Mach numbers of 0.0, 0.2, and 0.4 and acoustic source azimuthal mode orders ranging from zero to four with radial mode orders up to three.

Geometry

A plan view of the test facility is shown in Fig. 1. Dominant azimuthal modes generated by SMS propagate through the source measurement section and inlet coupler and radiate into the anechoic chamber from the inlet geometry under test. The air for the flow experiments is provided by a large compressor

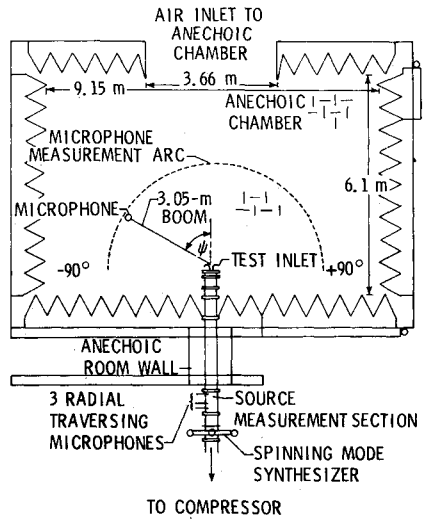

Fig. 1 Plan view of SMS/flow duct facility in Aircraft Noise Reduction Laboratory.

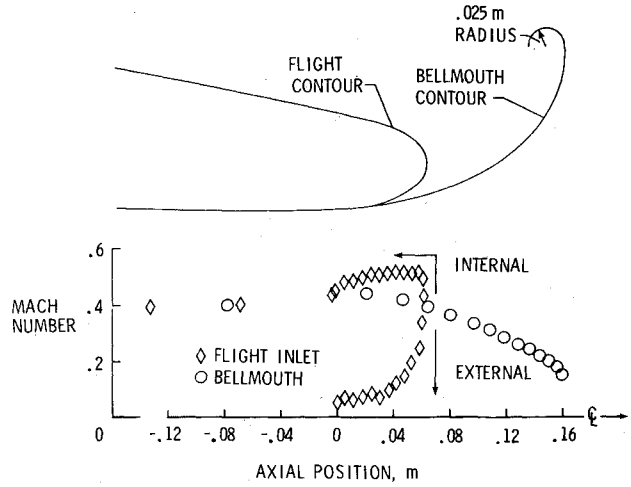

Fig. 2 Contours of two axisymmetric inlets tested and plot of experimentally derived wall Mach numbers vs axial position.

downstream of the flow duct utilizing the anechoic room as a plenum. Air is supplied to the anechoic room through a large supply duct on the rear wall. Subsequently, this air is drawn into the inlet and through the 0.3-m-diam flow duct.

The operation of the spinning mode synthesizer is given in detail in Refs. 2 and 9. The adjoining duct section is the source measurement section where the incident and reflected wave fields are defined. This section consists of three radial traversing microphones mounted on a rotating drum. The two upstream microphones are spaced from the downstream reference microphone by 0.159 and 0.365 m. An acoustic pressure measurement may be made at any point on these three cross sections. The radiated pressure was recorded from a continuously moving boom microphone traversed on a 3.05-m horizontal circular arc centered at the inlet highlight.

The inlet contours for the bellmouth and flight inlets are compared in Fig. 2. Both axisymmetric inlets terminated in the constant-area duct of 0.15-m radius which makes up the flow duct system. The bellmouth inlet geometry is a typical test inlet designed to provide good inflow characteristics in a static test configuration and is the bellmouth used in the work of Ref. 2. Its contour consists of a 1.43:1 ellipse, a highlight/diameter ratio of 1.75, and the interior radius is defined by

$$r_w = 0.262 - 0.112\sqrt{1.0 - (x/0.160)^2} \qquad 0.0 < x < 0.160$$
$$= 0.150 \qquad x < 0.0 \qquad (1)$$

with the origin on the duct axis at the beginning of the area expansion and all dimensions in meters.

The flight inlet geometry was taken from a flight effects study design and was found to be typical of current flight contours although it was also chosen to provide a relatively smooth inflow under static test conditions. The geometry is made up of a 2:1 ellipse faired smoothly to a conical section of 10.76-deg half-angle on the exterior cowl and joins the interior flow duct contour smoothly at $x = 0.0$. This flight inlet has a highlight/diameter ratio of 1.21 and is described by the following equation:

$$r_w = 0.181 \pm 0.031\sqrt{1.0 - (x/0.062)^2} \qquad 0.0 < x < 0.062$$
$$= 0.150 \qquad x < 0.0 \qquad (2)$$

The positive sign of the ellipse equation is taken for the exterior cowl and the minus sign for the interior contour. The overall lengths of the bellmouth and flight inlets from the highlight to the reference microphone in the source measurement section is 4.176 and 4.168 m, respectively.

Data Acquisition and Reduction

The data acquisition system consisted of the SMS system, the three microphones in the source measurement section and their associated positioning equipment, the far-field microphone and drive system, and an array of surface pressure taps and pitot probes to define the flowfield.

The SMS system is documented extensively in Ref. 9 and will not be repeated here. Similarly the source measurement hardware is documented in Ref. 10, with the same phase-averaging technique employed here. In Ref. 2 variations in the far-field data in the flow cases were attributed to small velocity fluctuations inducing variations in the radiated acoustic field. In order to alleviate this problem, which is associated with the short averaging time needed for a continuously moving boom, multiple sweeps of the boom microphone are provided. Phase-averaged data taken within each of 256 arc segments for each 180-deg sweep of the boom are displayed on a computer terminal. Data from successive boom sweeps are averaged together and repeatedly displayed as a test of convergence. For the no-flow results two sweeps were taken. For the flow cases, six to twelve sweeps were needed.

The aerodynamic data consisted of pitot tube traverses of the duct diameter and static pressure measurements of the surface pressures around the inlet contour of each geometry. Mach number and boundary-layer characteristics were calculated using standard compressible flow relations and the locations of the static taps are indicated by the data points in Fig. 2.

The in-duct data reduction technique assumed a modal representation of the duct pressure field in the following form:

$$p(r,\theta,x) = \sum_m \sum_n \left[A^+_{mn} e^{j\Omega^+_{mn}x} + A^-_{mn} e^{j\Omega^-_{mn}x} \right] J_m(\lambda_{mn} r)\, e^{jm\theta} \qquad (3)$$

where

$$\Omega^{\pm}_{mn} = \frac{+kM_0 \pm \sqrt{k^2 - (1 - M_0^2)\lambda^2_{mn}}}{1 - M_0^2} \qquad (4)$$

and M_0 is the average duct Mach number taken to be positive for flow into the inlet. The modal coefficients in Eq. (3), $A^{\pm}_{mn}$, are unknown and to be determined.

In order to determine these modal coefficients from the measured in-duct pressure field, the least-squares solution technique of Ref. 10 is used. In this work, however, the data acquisition procedure was refined to provide for an improved tracking of the modes of interest. This is accomplished by

observing the two data points per cycle criterion[10] for azimuthal modes and positioning radial measurements at the local peaks of the respective radial mode under consideration. In this way, the data measurement points were selected to give a well-conditioned set of equations from which to solve for the unknown modal coefficients.

The reflection coefficients presented in the results are computed from the mode coefficients as the magnitude of the complex ratio, A^-_{mn}/A^+_{mn}. The source amplitude of the incident wave is calculated by dividing the source mode pressure coefficient A_{mn} by the maximum peak of far-field sound pressure and expressing this on a logarithmic scale of normalized sound pressure level (SPL). As the radiation directivity is plotted with respect to a 0 dB peak level, the source strength is the magnitude of the source mode pressure coefficient relative to this 0 dB reference level.

Results and Discussion

The results of this work are presented in terms of the geometry and inlet flow effects on the duct termination condition and radiated field. The reflection coefficient for the most dominant mode, found to be the highest order propagating radial mode for the particular azimuthal mode being excited, is tabulated vs nondimensional frequency, ka. In general the particular mode of interest dominated the in-duct acoustic field by 10 to 25 dB with the maximum isolation occurring near the mode cutoff condition with decreasing isolation as the frequency was increased. The radiation data is presented as a normalized SPL plotted vs radiation angle, ψ in Fig. 1 from -90 to $+90$ deg. For an isolated mode, this directivity should be symmetrical about $\psi = 0$; however, due to the presence of extraneous modes yielding interference patterns and standing waves in the anechoic room, some deviations of symmetry will be noted. The amplitude is plotted such that the peak level of the stronger radiation pattern is referenced as 0 dB. The level of the corresponding amplitude plot is adjusted to give the correct relative amplitude between the cases presented. In addition, the source strength, defined in the previous section, is given, relative to the 0 dB level of the radiation plot.

Table 1 Comparison of reflection coefficient moduli for spinning mode order 1

Mode				$\lvert R\rvert$		
m	n	ka	ξ	Bellmouth inlet	Flight inlet	Unflanged duct
1	0	1.86	1.01	—	0.69	—
1	0	1.91	1.04	0.55	0.63	0.84
1	0	2.06	1.12	0.36	0.50	0.58
1	0	2.25	1.22	0.22	0.45	0.65
1	0	2.66	1.44	0.16	0.29	0.50
1	0	3.20	1.74	—	0.16	—
1	0	3.76	2.04	0.07	0.10	0.27
1	0	5.29	2.87	0.04	0.11	0.11
1	1	5.54	1.04	0.20	0.37	—
1	1	5.92	1.11	0.24	0.20	—
1	1	6.50	1.22	0.09	0.07	—
1	1	7.68	1.44	0.02	0.07	—
1	2	9.28	1.09	0.11	0.22	—

Table 2 Comparison of reflection coefficient moduli for spinning mode order 4

Mode				$\lvert R\rvert$		
m	n	ka	ξ	Bellmouth inlet	Flight inlet	Unflanged duct
4	0	5.37	1.01	—	0.93	—
4	0	5.51	1.04	0.30	0.25	0.73
4	0	5.81	1.09	0.10	0.11	0.41
4	0	6.49	1.22	0.02	0.14	0.34
4	0	7.66	1.44	0.04	0.04	0.17
4	0	9.19	1.73	0.07	0.08	—
4	1	9.65	1.04	0.09	0.11	—
4	1	10.30	1.11	0.19	0.22	—
4	1	11.32	1.22	0.14	0.07	—
4	2	13.37	1.05	0.17	0.13	—

Geometry Effects on Acoustic Reflections

A comparison of the measured reflection coefficient $|R|$ for both inlets is given in tabular form in Tables 1 and 2 for the first and fourth azimuthal mode orders, respectively, for no mean flow. In Table 1, the effects of geometry on the modulus of the reflection coefficient is shown for an azimuthal mode of order 1. In addition to the bellmouth and flight inlet results, unflanged or abruptly terminated duct data from Ref. 2 is also presented for the lowest order radial mode. As shown, the reflection coefficient decreases dramatically in amplitude from values approaching unity near the mode cutoff condition to values of 0.1 or less at $ka = 4$ for the contoured inlets and lowest order radial mode. In this case, the magnitude of the reflection coefficient for the bellmouth near cutoff is 50-85% that of the flight inlet and 30-65% that of the unflanged duct. At a cutoff ratio of 2.9 or $ka = 5.29$ the reflection characteristics are nearly identical for this lowest order mode. The data shown for the (1,1) mode exhibits a similar trend except for one anomalous point for the bellmouth geometry at $ka = 5.54$. Note that for identical cutoff ratios, the second-order radial mode exhibits considerably lower reflection coefficient amplitudes than the lowest order radial mode. For example, the (1,0) mode reflection coefficient moduli at $ka = 1.91$ and 2.06 for the flight inlet are 0.63 and 0.50. The (1,1) mode at $ka = 5.54$ and 5.92 but identical cutoff ratios exhibit reflection coefficients of 0.37 and 0.20, respectively. The bellmouth geometry follows the same trend although the differences are not as dramatic due to the lower overall coefficient magnitude. For this azimuthal mode and the contoured inlets, the magnitude of the reflection coefficient has dropped to levels of 0.1 at a cutoff ratio of 2.04 ($ka = 3.76$) for the lowest order radial mode and a cutoff ratio of 1.22 ($ka = 6.50$) for the higher order radial mode. Thus, it can be seen that in addition to the cutoff ratio dependence, the reflection coefficient is also strongly dependent on the overall frequency or ka. Also, the differences between the two geometries are seen to diminish for the higher order radial source.

Similar relative magnitudes and trends between the inlet geometries and source mode orders were found for the azimuthal mode of order 2. For this case, the reflection coefficient moduli converge to limiting values at cutoff ratios of 1.73 ($ka = 5.29$) and 1.22 ($ka = 8.18$) for the (2,0) and (2,1) modes, respectively.

Table 2 displays similar results for the fourth-order azimuthal mode. Here, as in the previous cases, the reflection coefficients for both contoured inlets are significantly lower in amplitude than the unflanged duct of Ref. 2. The bellmouth data, while generally less than that of the flight data, have fairly well collapsed to show very little geometry effect away from cutoff. Both contoured inlets have reflection coefficient amplitudes that converge to 0.1 at a cutoff ratio of 1.09 ($ka = 5.81$), indicating that the compression of geometry effects into lower values of cutoff ratio shown in the previous case for higher order radial modes also applies for this lowest order radial mode. Note that this effect for the (4,0) mode occurs in the same frequency range as for the (1,1) mode of Table 1. The data for the (4,1) mode also indicate that the geometry effect has become negligible, although, at this higher frequency and low values of reflection coefficient, more confidence must be placed in the trend of the data than in the absolute value.

Geometry Effects on Acoustic Radiation

Figure 3 presents the normalized radiation directivity vs the radiation angle ψ for the bellmouth and flight inlets with a (1,0) mode incident. Nondimensional frequency ka is 2.06 and the reference source strength is 40.5 dB. The symmetric single-lobed pattern is characteristic of this (1,0) mode, thus indicating that this single mode is the dominant acoustic mode present. The levels of the two curves are corrected to the same source strength and the comparison shows a 3-4 dB higher level for the bellmouth inlet due to the decreased reflection that occurs for this geometry. Also note the difference in directivity characteristics for the two inlet geometries. The bellmouth focuses its peak radiation toward the centerline at 35 deg, whereas the flight inlet radiates to significantly larger angles, 55-60 deg from the duct centerline. Thus, for sound radiated at these higher angles, which have proportionately shorter paths to ground receivers, the levels are quite comparable although the peak levels of the bellmouth are significantly higher.

A similar comparison at a slightly higher frequency, $ka = 2.66$, is shown in Fig. 4. The source strength is 34.1 dB indicating a greater radiation efficiency over the previous case. Also, the peak flight inlet levels are down by less, about 2.5-3 dB, from the bellmouth peak levels due to the decreasing difference in the reflection coefficient. The radiation directivity of both contoured inlet geometries are redirected more toward the duct axis with the bellmouth radiating peak levels at 30 deg and the flight inlet at 47 deg from the duct axis. For comparison, an unflanged duct radiation directivity from Ref. 2 is shown for comparison with an arbitrary offset of 10 dB.

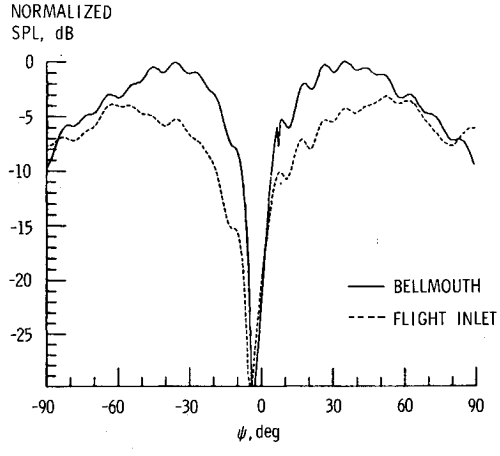

Fig. 3 Influence of inlet geometry on far-field sound pressure for an incident (1,0) mode with $ka = 2.06$.

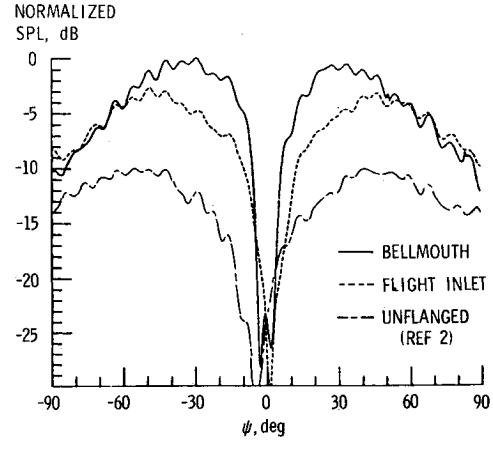

Fig. 4 Influence of inlet geometry on far-field sound pressure for an incident (1,0) mode with $ka = 2.66$.

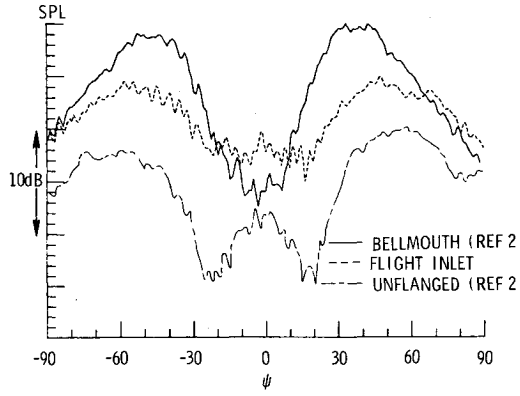

Fig. 5 Influence of inlet geometry on far-field directivity for an incident (4,0) mode with $ka = 5.81$.

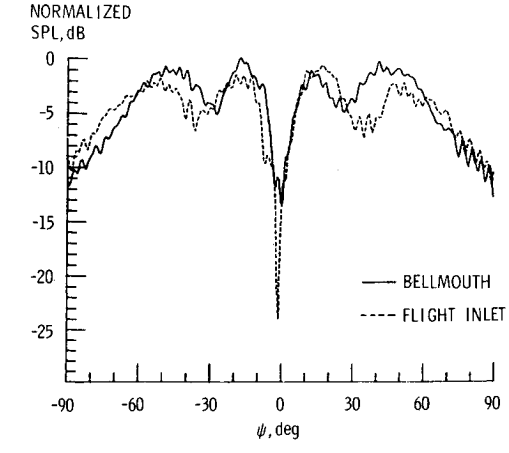

Fig. 6 Influence of inlet geometry on far-field sound pressure for a dominant (1,1) mode with $ka = 5.92$.

The directivity of these data peaks at about the same angular position as the flight inlet data although it is more broad since it does not fall off as much at higher angles.

Figure 5 shows the radiation directivities of the same three inlet geometries as the previous figure but for a ka of 5.81 and a (4,0) mode incident. Here both the bellmouth and unflanged duct data were taken from the results of Ref. 2 for which absolute source strengths were not available. Therefore, the flight inlet and unflanged duct data are arbitrarily offset 5 and 10 dB, respectively, from the bellmouth peak levels. The point to be made is that the effect of geometry on the angle of peak radiation at this higher frequency is significantly less than that shown in Fig. 3 for the (1,0) mode at an identical cutoff ratio ($\xi = 1.1$). In Fig. 5, the bellmouth radiates peak levels at angles of 41 deg and the flight inlet radiates peak levels about 50 deg from the duct axis. This difference of 9 deg compares to 25 deg for the (1,0) mode at $ka = 2.06$. The unflanged duct radiates peak levels about 8 deg wider than the flight inlet at this decreased cutoff ratio compared to that of Fig. 4.

Figure 6 compares the normalized radiation directivity of the bellmouth and flight inlets for a (1,1) mode at a normalized source strength of 38.3 and a (1,0) mode at 28.6 dB in combination for a nondimensional frequency of 5.92 and a cutoff ratio of 1.1. Here the peak levels differ by only 1 dB due to the modulus of the reflection coefficient being nearly equal. The directivity is dominated by the dual-lobed symmetric pattern of this higher order radial mode. The angular locations of the inner and outer lobes differ by only 5 and 7 deg, respectively.

As a final illustration of the comparison of the geometries tested Fig. 7 shows the normalized radiation directivities for a (2,2) mode at 35.3 dB, a (2,1) mode at 19.3 dB, and a (2,0) mode at 9.5 dB incident at a nondimensional frequency of

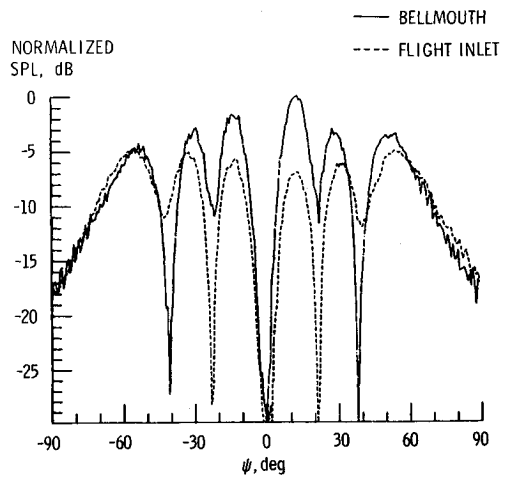

Fig. 7 Influence of inlet geometry on far-field sound pressure for a dominant (2,2) mode with $ka = 11.67$.

11.67. For a cutoff ratio of 1.17, where geometry effects would be expected to be very strong, the data indicate nearly identical directivity patterns. The difference in level indicates a stronger internal reflection for the flight inlet although the reflection coefficient data does not show the necessary difference.

The above data in the acoustic far field indicate that, as with the in-duct data, the geometry-induced effects compress into cutoff ratios closer to unity as the absolute frequency is increased. This suggests that a parameter comparing the free space wavelength to the inlet lip thickness or contraction ratio may come into play. Remember that the data differences due to geometry effects of the thin-lipped unflanged duct (a limiting geometric case) compared to the two contoured geometries persisted at much higher frequencies. Projecting this result to practical applications in turbofan inlets at high ka, geometry effects arising from static test inlets vs flight hardware may be negligible except at frequencies very near mode cutoff. Close to cutoff, the internal reflection due to the presence of the diffuser contraction (see Ref. 10) may make this range of frequencies unimportant for inlet geometry considerations also.

Mean Flow Effects

Measurements of the internal and radiated acoustic fields for azimuthal mode orders 1 and 2 were made for Mach numbers of 0.2 and 0.4. In addition, static wall pressures and pitot tube traverses of the duct diameter were made to define the mean flow. Referring to Fig. 2, plots of the wall Mach number calculated from wall static pressures are given for both inlets at their proper relative axial position. The bellmouth inlet exhibits a gradual acceleration of the flow from highlight to throat where the flow steadies out to a uniform Mach 0.4 flow as indicated by a pitot tube traverse at $x = -0.67$ m. Except in local regions external to the highlight and at the beginning of the constant-area section, this geometry would be expected to produce a nearly one-dimensional flowfield. In contrast, the inlet flow of the flight contour contains strong radial and axial gradients. Examination of the flight inlet flow data shows a strong acceleration of the flow around the highlight and a subsequent deceleration into the constant-area section. This effect is due to the proximity of the inlet wall. The centerline Mach number would show a strong monotonic axial acceleration of the flow from the highlight to throat. Therefore, acoustic refraction effects due to these flow gradients would be expected to be stronger with the flight inlet. Pitot tube traverses of the in-duct flow reveal a uniform flow core with boundary-layer thicknesses of 19 mm for the bellmouth and 13 mm for the flight geometry at 0.4 Mach number.

Flow Effects on Acoustic Reflections

Table 3 shows the effect of flow on the amplitude of the pressure reflection coefficient of the flight inlet for azimuthal mode orders 1 and 2. Consistent with the results of Ref. 2 for the bellmouth, the flow lowers the amplitude of the reflection by effectively increasing the mode cutoff ratio. The effect is most drastic near mode cutoff with decreases of 50% and smaller decreases as ka is increased above the cutoff condition. The effect of the flow on the higher order radial modes was to decrease the reflected wave amplitudes to indistinguishable levels.

In addition to the above effect on the pressure reflection coefficient, the flow also has a convective effect on the incident and reflected acoustic intensity flux. The flow opposes the incident or transmitted acoustic field and therefore causes a decrease in the incident acoustic intensity for the same source strength since the source strength is defined in terms of pressure. For identical source strengths and pressure reflection amplitudes, a case with opposing flow will radiate significantly less energy because the incident energy is less. In the acoustic far field where the flow is negligible the acoustic pressure, being proportional to the square root of the acoustic intensity, will be reduced over a case without internal flow. This effect opposes the demonstrated reduction in reflection coefficient modulus and for some cases results in radiated levels for the flow cases being less than the radiated levels for the no-flow cases.

Flow Effects on Acoustic Radiation

Figure 8 compares the Mach 0.4 flow and no-flow radiated pressures vs radiation angle for a (1,0) mode at a fixed nondimensional frequency of 1.91. Here, the decrease in reflection coefficient and flow convective effect are nearly offsetting and result in comparable radiated levels. More important, though, for this no-flow cutoff ratio of 1.04 there is little effect

Table 3 Effect of flow on reflection coefficient moduli for the flight inlet

Mode			ξ		$\lvert R\rvert$	
m	n	ka	$M=0$	$M=0.4$	$M=0$	$M=0.4$
1	0	1.91	1.04	1.13	0.63	0.34
1	0	2.06	1.12	1.22	0.50	0.38
1	0	2.25	1.22	1.33	0.45	0.29
1	0	3.20	1.74	1.90	0.16	0.07
2	0	3.16	1.03	1.13	0.67	0.33
2	0	3.37	1.10	1.20	0.40	0.32
2	0	3.72	1.22	1.33	0.26	0.19
2	0	4.46	1.46	1.59	0.19	0.23

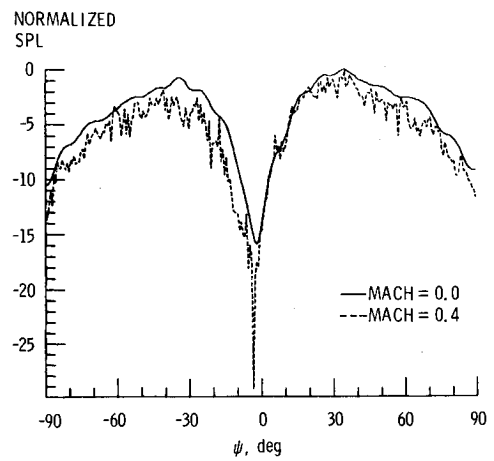

Fig. 8 Influence of flow on the far-field sound pressure radiated from the bellmouth inlet for a (1,0) mode incident at 40.5 dB and $ka = 1.91$.

of the flow on the directivity of the radiated field. Similar results for this configuration with higher order modes are given in Ref. 2.

Figures 9 and 10 show the effects of the Mach 0.4 flow on the radiated field of the flight inlet geometry. It was expected that the strong spatial mean flow gradients pointed out earlier for the flight inlet would affect the radiated field more than that found for the bellmouth inlet. It had also been thought that the rather long and slowly expanding contour of the bellmouth may have allowed internal reflections that masked the effects of inflow on the acoustic radiation directivity. These two figures, typical of all of the available data, point out that this is not the case. Figure 9 shows the effect of flow on the radiated field for a (1,0) mode at a nondimensional frequency of 2.06. Figure 10 gives the results for a (2,0) mode incident at a ka of 3.72. In both cases the radiation directivity remained virtually unchanged. However, the difference in levels of Fig. 9 is not clearly understood. The greater decrease in reflection coefficient amplitude offsetting the convective effect of the flow for this case over that of Fig. 10 should result in closer agreement in absolute levels for the case of Fig. 9.

As a final demonstration of the insensitivity of the radiated directivity on the mean flow, Fig. 11 shows the normalized directivity of a combination (2,1) mode at 32.6 dB and a (2,0) mode at 25.6 dB source strength radiating from the bellmouth inlet for a Mach 0.2 and no-flow condition. The nondimensional frequency of 8.18 gives a no-flow cutoff ratio of 1.22. Again, the radiation directivity of the flow case shows virtually no deviation from that of the no-flow case. For this higher frequency little change in the net transmitted acoustic field is made by the change in reflection coefficient so that the difference in levels is dominated by the convected energy effect resulting in the reduced overall levels for the flow case.

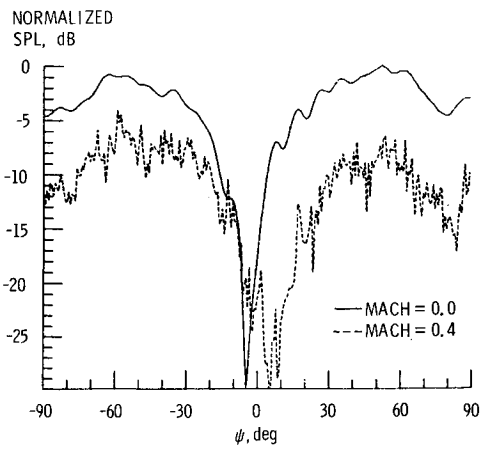

Fig. 9 Influence of flow on the far-field sound pressure radiated from the flight inlet for a (1,0) mode incident at 39.9 dB and $ka = 2.06$.

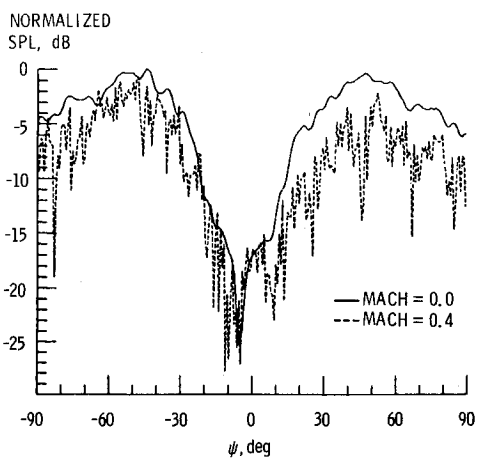

Fig. 10 Influence of flow on the far-field sound pressure radiated from the flight inlet for a (2,0) mode incident at 40.2 dB and $ka = 3.72$.

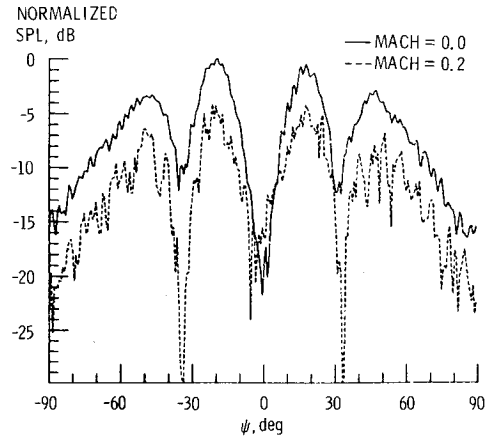

Fig. 11 Influence of flow on the far-field sound pressure radiated from the bellmouth inlet for a dominant (2,1) mode.

Concluding Remarks

An experiment was conducted in the NASA Langley spinning mode synthesizer/flow duct facility to study the reflection and radiation characteristics of individual duct modes from realistic static and flight-type turbofan inlets. Measured test data were resolved into reflection coefficients and absolute radiated sound pressure directivities. Comparisons are drawn showing the effects of inlet geometry, static inflow, frequency, and incident mode structure on the above quantities.

In considering the geometry effects, this study confirms the results of a previous study that the in-duct reflection decreases and the radiated levels peak at successively closer angles to the duct axis with increasing cutoff ratio. In addition, evidence is presented suggesting that the strong effects of geometry on the reflected and radiated acoustic fields diminish with increasing absolute frequency. That is to say that the effects of geometry become more concentrated near the mode cutoff condition at higher frequencies. Therefore, at practical engine operating conditions the geometry effect of the inlet may not be important.

The effect of static inflow on the radiated directivity has been found to be negligible for a fixed incident mode and nondimensional frequency. This was found to be the case for both the bellmouth inlet and the flight inlet, even though the latter exhibited much stronger geometric and flow gradients. The effect of the flow on the internal acoustic field is to lower the magnitude of the reflection coefficient significantly for those cases near mode cutoff. Also due to the convective effect the net radiated energy for a constant source pressure is reduced.

In addition, it was found that the higher order radial modes display much the same characteristics as do the lowest order radial modes. However, the higher frequencies at which these modes propagate lessen the geometry and frequency effects at comparable cutoff ratios.

References

[1]Rice, E.J., Heidmann, M.F., and Sofrin, T.G., "Modal Propagation Angles in a Cylindrical Duct with Flow and their Relation to Sound Radiation," AIAA Paper 79-0183, Jan. 1979.

[2]Ville, J.M. and Silcox, R.J., "Experimental Investigation of the Radiation of Sound from an Unflanged Duct and a Bellmouth Including the Flow Effect," NASA TP-1697, Aug. 1980.

[3]Clark, T.L., Slotboom, D.R., and Vaidya, P.G., "Investigation of the Effects of Inlet Shapes on Fan Noise Radiation," NASA CR-3416, April 1981.

[4]Horowitz, S.J., Sigman, R.K., and Zinn, B.T., "An Iterative Finite

Element-Integral Technique for Predicting Sound Radiation from Turbofan Inlets in Steady Flight," AIAA Paper 82-0124, Jan. 1982.

[5]Eversman, W. and Astley, R.J., "Wave Envelope and Infinite Element Schemes for Fan Noise Radiation from Turbofan Inlets," AIAA Paper 83-0709, April 1983.

[6]Preisser, J.S. and Chestnutt, D., "Flight Effects on Fan Noise with Static and Wind Tunnel Comparisons," AIAA Paper 83-0678, April 1983.

[7]Andersson, A.O., "Boeing Experience: Session I—ICD Experience and Design Criteria," *Flight Effects of Fan Noise*, NASA CP-2242, Jan. 1982, pp. 11-13.

[8]Baumeister, K.J. and Horowitz, S.J., "Finite Element-Integral Simulation of Static and Flight Fan Noise Radiation from the JT15D Turbofan Engine," NASA TM-82936, Nov. 1982.

[9]Palumbo, D.L., "An Operations Manual for the Spinning Mode Synthesizer in the Langley Noise Reduction Laboratory," NASA CR-165698, March 1981.

[10]Silcox, R.J. and Lester, H.C., "Sound Propagation Through A Variable Area Duct: Experiment and Theory," *AIAA Journal*, Vol. 20, Oct. 1982, pp. 1377-1384.